Fully-Propulsive Mars Atmospheric Transit Strategies for High-Mass Missions

Space Systems Design Laboratory (SSDL)
Guggenheim School of Aerospace Engineering
Georgia Institute of Technology
Atlanta, GA

Author:
ENS Christopher L. Marsh, USN

Advisor:
Dr. Robert D. Braun

April 29, 2009

Fully-Propulsive Mars Atmospheric Transit Strategies for High-Mass Missions

Christopher L. Marsh
Georgia Institute of Technology, Atlanta, Georgia, 30332

Robert D. Braun
Faculty Advisor, Georgia Institute of Technology, Atlanta, Georgia, 30332

A systems analysis focused on the use of propulsion during the EDL sequence at Mars for high-payload missions is presented. Trajectory simulation and mass sizing are performed to analyze the feasibility of a fully-propulsive descent. A heat rate boundary and associated control law are developed in an effort to limit the heating loads placed on the vehicle. Analysis is performed to explore the full-propulsive EDL strategy's sensitivity to the vehicle's propulsive capabilities and aero-propulsive and vehicle models. The EDL strategy is examined for ranges of initial masses and heat rate constraints, outlining an envelope of feasibility. The proposed architecture is compared against EDL systems in which significant aeroassist technology is employed. With this information, an overview of the impact of a fully-propulsive EDL system on spacecraft design and functionality is offered.

Nomenclature

ΔV = change in velocity, km/sec^2
T_{max} = maximum thrust, N
I_{sp} = specific impulse, sec
$\dot{m}$ = time derivative of mass, kg/sec
g_0 = Earth gravitational accel., m/sec^2
T/W = thrust-to-weight
m_{engine} = engine mass, kg
C_T = thrust coefficient
$\bar{q}$ = dynamic pressure, Pa
A = reference area, m^2
k_{C_D} = drag coefficient multiplier
m_{FBS} = forebody structure mass, kg
$\bar{q}_{max}$ = maximum dynamic pressure, Pa
$\dot{q}_{conv}$ = convective heat rate, W/cm^2
ρ = atmospheric density, kg/m^3
r_n = vehicle nose radius, m
v_{rel} = planet relative velocity, m/sec^2
m_{TPS} = thermal protection system mass, kg
$q_{conv,total}$ = integrated convective heat load, J/cm^2
$m_{payload}$ = payload mass, kg
m_{landed} = landed mass, kg
$m_{prop\ sys}$ = propellant system mass, kg
$m_{RCS\ sys}$ = reaction control system mass, kg
$m_{backshell}$ = backshell mass, kg
h = altitude, m
V = velocity, m/sec
ε = emissivity
$V_{rel,con}$ = constraint relative velocity, m/sec
D = drag, N
$k_{structure}$ = structural mass multiplier

I. Introduction

The United States has safely landed six spacecraft on Mars starting with Viking 1 and 2 in 1976 and continuing to the recently landed Phoenix. However, the largest landed mass of these missions is 590 kg.[1] While NASA is currently preparing for flight of the Mars Science Laboratory and its 900 kg landed payload,[2] the Vision for Space Exploration calls for eventually sending humans to Mars with landed masses in range of 40 to 80 metric tons.[3] One of the most significant challenges of a human Mars mission is in the area of entry, descent, and landing (EDL). Due to the presence of a thin but significant atmosphere at Mars, current Mars EDL strategies and technologies depend heavily on aerodynamic forces to slow the vehicle. These concepts are largely derived from Viking and Earth-return experience. However, this proven technology does not allow for extension of landed mass capability to the level required for human exploration.[1] As an example, NASA's previous Design Reference Mission[4] required a cluster of

three 50-m diameter Viking heritage parachutes to be deployed supersonically. This requirement is likely well beyond the supersonic disk-gap-band parachute capability.

Due to the low density of the Mars atmosphere (approximately 1/100th as dense as Earth's), a Mars landing architecture comparable to that used in human exploration of the Moon is a natural consideration. In the Apollo program, propulsion was employed in the descent and landing sequence, where the lunar landers' propulsion system provided all of the ΔV required from lunar orbit to landing. Although not the main contributor in the EDL system, propulsion has been used in several robotic missions to Mars. A summary of the use of propulsion in the lunar and Mars landings is given in Table 1.[1,5-15] The capabilities required by human Mars exploration greatly surpass those outlined in Table 1.

Table 1 Historic Uses of Propulsion in EDL[1,5-15]

	Apollo	Viking 1/2	MPF	MER-A/B	Phoenix	MSL
Use of propulsion	lunar deorbit and landing	terminal descent	terminal descent and flyaway	terminal descent and flyaway	terminal descent	terminal descent and flyaway
Propellant type	N_2O_4/A-50	hydrazine	solid rockets	solid rockets	hydrazine	hydrazine
ΔV imparted, m/s	2010	220	63	57.4/61.8	55.3	120
Maximum thrust, kN	43.9	8.0	23.8	23.3	30.3	24
Throttling	10 - 60% of T_{max}	10:1	none	none	off-pulsed	13 - 100% of T_{max}
$I_{sp,}$ sec	311	210	260	273.9	212.5	210
Mass of propellant, kg	8165	185	20.7	27.1	37.4	340
Total mass of engines, kg	113	23	30.7	17.5	30	72
Landed mass, kg	7000-8250	590	360	539	382	900

This paper investigates the ability to employ a fully-propulsive atmospheric transit strategy at Mars for high-mass payload missions. The objective of this systems analysis effort is to provide a fully-propulsive reference architecture for comparison with EDL architectures that employ aeroassist technology. In this study, fully-propulsive descent refers to deceleration sequences that do not include aeroassist technology elements such as lifting aeroshell configurations, ablative thermal protection systems, parachutes, or inflatable aerodynamic decelerators (IAD). Instead, these architectures consist of powered flight from Mars orbit or hyperbolic approach conditions to the surface in which deceleration is achieved through a combination of propulsive thrust and aerodynamic drag. The study explores the potential of avoiding heating constraints by altering the vehicle's deceleration. Propulsive strategies considered include a constant-thrust gravity turn as well as variable-thrust trajectory designs. This study examines the fully-propulsive architecture requirements as well as the architecture's sensitivities. Finally, the current EDL strategy is incorporated into high-mass mission architecture.

II. Approach

A. Simulation

To perform the necessary studies, a MATLAB-based entry simulation was created to propagate the three degree-of-freedom translational equations of motion from a given set of initial conditions until termination at the surface of the planet. The simulation models a spherical, rotating planet with forces due to gravity, thrust, and drag. The vehicle follows a ballistic trajectory and does not take advantage of aerodynamic lift. The vehicle used in the study is a 70° sphere-cone similar to that used by the robotic missions referenced in Table 1. The simulation uses a tabulated coefficient of drag as a function of Mach number and interpolates between data points. The reference atmosphere used is tabulated from the Mars Pathfinder mission.

Simulation validation is critical to ensure the accuracy of the results of this study. To do so, a Mars Pathfinder simulation was compared against a trajectory of the same mission simulated with the Program to Optimize Simulated Trajectories (POST).[16] As shown in Fig. 1 and Table 2, the trajectory generated by the MATLAB entry

simulation is in excellent agreement with the POST trajectory. Position, velocity, flight path angle (FPA), dynamic pressure, heating, and g-load calculations were validated through this process.

Table 2 Event Comparison for Trajectory Validation

Event	This Study	POST	Difference (%)
Entry			
Time (sec)	0	0	0.00
Altitude (m)	128000	128000	0.00
Relative Vel. (m/sec)	7479	7479	-0.01
Relative FPA (º)	-13.65	-13.65	0.00
Parachute Deploy			
Time (sec)	154.5	154.5	0.00
Altitude (m)	9916	9916	0.00
Relative Vel. (m/sec)	414.5	414.5	0.01
Relative FPA (º)	-23.35	-23.35	-0.01
Dyn. Pressure (Pa)	585.0	585.0	0.00
Heatshield Jettison			
Time (sec)	174.5	174.5	0.00
Altitude (m)	8217	8219	-0.03
Relative Vel. (m/sec)	90.36	90.23	0.14
Relative FPA (º)	-47.29	-47.33	-0.08
Dyn. Pressure (Pa)	32.07	31.98	0.30
Trajectory Termination			
Time (sec)	359.8	359.8	0.01
Altitude (m)	-2408	-2408	0.00
Relative Vel. (m/sec)	42.64	42.64	0.01
Relative FPA (º)	-89.88	-89.88	0.00
Dyn. Pressure (Pa)	21.55	21.55	-0.02

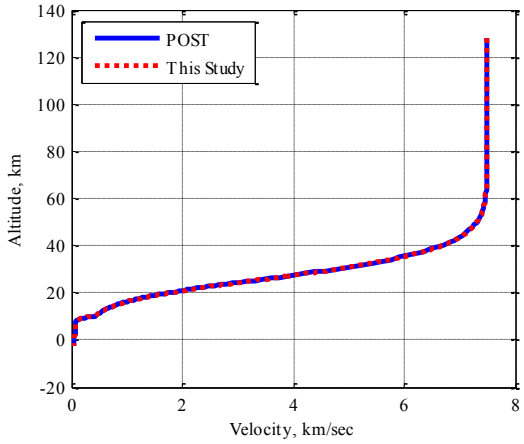

Fig. 1 Trajectory Validation

The simulator has the ability to use various thrust control modules. These modules specify the thrust direction and magnitude throughout the trajectory. The thrust control module and the mass impact of the use of thrust were validated against an independent simulation used in a recent assessment of Mars pinpoint landing performance.[17] A Newton-based solver is used within the simulator to calculate the altitude at which to begin the constant-thrust gravity turn as to ensure a velocity of less than 0.1 m/sec at landing. Fig. 2 and Table 3 show the excellent agreement between trajectory parameters for the constant-thrust gravity turn validation case.

Table 3 Event Comparison for Propulsive Maneuver Validation

Event	This Study	Secondary Simulation[17]	Difference
Ignition			
Time (sec)	0.00	0.00	0.00
Mass (kg)	9713.24	9713.24	0.00
Altitude (m)	14885.40	14885.40	0.00
Relative Vel. (m/sec)	1902.73	1902.73	0.00
Relative FPA (°)	-6.38	-6.38	0.00
Trajectory Termination			
Time (sec)	95.36	95.36	0.00
Mass (kg)	6615.61	6615.71	0.10
Altitude (m)	0.00	0.17	0.17
Relative Vel. (m/sec)	0.07	0.10	0.03
Relative FPA (°)	-82.36	-81.41	0.95

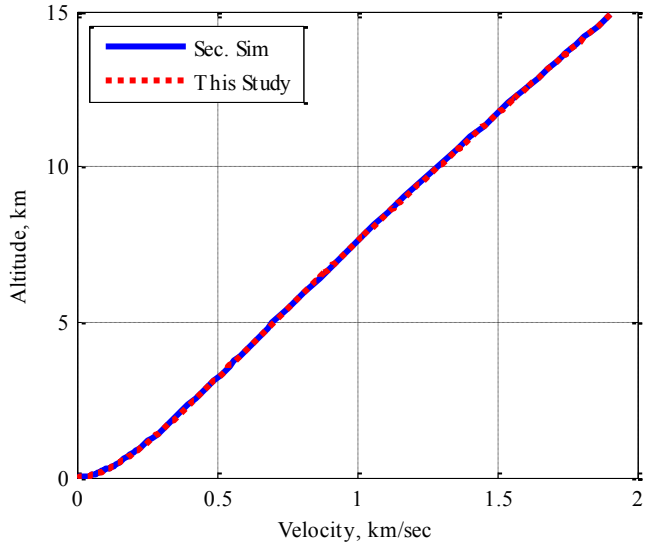

Fig. 2 Propulsive Maneuver Validation[17]

B. Modeling

Throughout the study, vehicle performance is based largely on the ability to deliver payload to the Mars surface. Therefore, modeling the vehicle's mass is a crucial aspect of the study. The vehicle's initial mass is broken into four general categories: propulsion and reaction control systems, thermal protection system (TPS), structure, and payload. A majority of the mass model is based on the work of Steinfeldt, et al.[19] such that a comparison to recent aeroassist technology studies may be performed.

1. Propulsion and Reaction Control Systems

The main component of the propulsion system mass is the propellant required for descent and landing. This value is calculated throughout the simulation as a part of the vehicle state as shown in Equation 1. Since there are no mass drops during the fully-propulsive trajectories provided in this study, the propellant required by a specific trajectory is calculated by subtracting the landed mass from the vehicle's initial mass.

$$\dot{m} = T \Big/ I_{sp} g_0 \tag{1}$$

In systems level studies, I_{sp} is generally determined through the type of fuel used. As in most previous human Mars exploration studies, the reference propellant assumed is LOX/CH_4. This choice is based largely on the ability to produce methane while on the surface of Mars and the need for commonality in the Earth-Mars and Mars-Earth

transportation systems required for human exploration.[4,19] The reference case of this study assumes an I_{sp} of 350 sec, although the system's sensitivity to I_{sp} is also provided. The vehicle's thrust, T in Equation 1, is assigned by the controller and is limited in magnitude by a specified thrust to weight ratio (T/W).

In the reference case, a constant-thrust gravity turn is used for the terminal segment of the EDL sequence. Gravity turns of the same ΔV require less fuel for increasing thrust levels. Theoretically, gravity turns are most efficient if employed with infinite thrust at the instant before touchdown. Fig. 3 shows that a mass savings of more than 15% can be realized if full throttle is used instead of a throttle setting of 50% for a vehicle with the capability of producing a thrust of 670 kN. These results are specific to the T/W and I_{sp} of the vehicle, however, they reflect the significant losses that can be incurred by low thrust maneuvers.

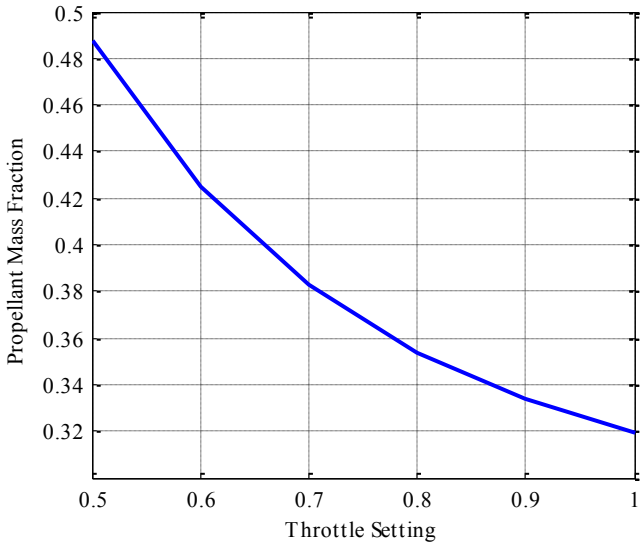

Fig. 3 Propellant Mass Fraction of a Terminal Gravity Turn Performed at Various Throttle Settings for a 60 mT, 10 m Diameter Vehicle

As such, in this investigation, the terminal gravity turn maneuvers utilize the maximum allowable thrust set by a wet vehicle thrust to weight ratio. The assigned thrust to weight ratio is based on the initial weight of the vehicle at Mars. The thrust is determined through this manner so that engine capability is scaled with the size of the vehicle. Previous studies have used T/W ratios ranging from 2 to 5.[19] The reference case in this study uses a T/W of 3. The sensitivity to this parameter is explored later.

In modeling the mass of the engines, it is necessary to specify the quantity of engines required and the mass of each engine. Individual engines are scaled according to the following relationship:

$$m_{engine} = 0.00144T + 49.6 \tag{2}$$

where T is the engine thrust in N and m_{engine} is the engine mass in kg. The relationship was developed by Christian, et al. through regression analysis of data for conceptual LOX/CH_4 engines.[19] The upper bound of the thrust of the engines used in forming the relationship was 200 kN.[20] In determining the mass of the engines for the current study, the thrust produced by a single engine is limited to this value. Limiting the maximum thrust that a single engine can produce and specifying the required total thrust of the propulsion system dictates the minimum number of engines on the vehicle. However, more consideration of the number and placement of engines is necessary.

It has been shown that individual engines placed in the center of the body can effectively eliminate the drag of the vehicle; whereas, placing engines at the periphery of the vehicle can preserve the vehicle's aerodynamic drag for thrust coefficients (defined in Equation 3) lower than one.[21]

$$C_T = T \big/ \bar{q}A \tag{3}$$

In an effort to model the aero-propulsive effects, a drag coefficient multiplier is defined through the linear piecewise function presented in Equation 4. The model was developed using available data for a 60° sphere-cone with a peripheral retropropulsion configuration thrusting into a Mach 2 freestream.[22] The model reflects preservation of drag for thrust coefficients lower than 1, degraded drag between thrust coefficient values of 1 and 3, and complete elimination of drag with thrust coefficient values greater than 3. The system's sensitivity to aero-propulsive effects is revisited later in the report.

$$k_{C_D} = \begin{cases} 1 - 0.0849 C_T & C_T \le 1.036 \\ 1.866 - 0.921 C_T & 1.036 < C_T \le 1.643 \\ 0.78 - 0.26 C_T & 1.643 < C_T \le 3 \\ 0 & 3 < C_T \end{cases} \tag{4}$$

Assuming sufficient throttling authority, additional engines also allow for engine-out capabilities thus increasing the system reliability. For these reasons as well as the aerodynamic benefits, the vehicles in this study have no less than four engines situated on the periphery of the vehicle's body.

Due to the heavy reliance on propulsion for deceleration in the current EDL architecture, the mass of the vehicle's propellant tanks is significant. For this study, the propellant tanks are sized according to the volume of propellant needed for the trajectory. An oxidizer to fuel ratio of 3.5 is assumed with the density of the methane and liquid oxygen to be 422.6 kg/m^3 and 1140.1 kg/m^3 respectively. The tanks are assumed to be made of titanium with an operating pressure of 1.4 MPa.[23]

Throughout the entry trajectory, it is assumed that attitude control is performed by a reaction control system (RCS). The mass of the RCS hardware is modeled as 0.5% of the vehicle's initial mass. The RCS propellant mass is calculated based on a ΔV requirement of 30 m/sec and an RCS I_{sp} of 200 sec. This method of modeling is consistent with previous high-mass Mars conceptual studies.[18,19]

2. Structure

To capture trajectory effects on the vehicle's structural mass, a relationship based on peak dynamic pressure was used to size the forebody's underlying structure. The relationship was formulated through regression analysis of previous robotic and human entry missions and is provided in Equation 5.[18]

$$m_{FBS} = m_0 \cdot 0.0232 \left(\bar{q}_{\max} \right)^{0.1708} \tag{5}$$

Referencing historical and conceptual robotic and crewed vehicles, Steinfeldt, et al. conservatively estimated the backshell mass as 14% of the vehicle's initial mass. The current study models backshell mass in the same manner. The forebody structure and backshell are combined to provide the vehicle's total structural mass.

3. Thermal Protection System

During atmospheric entry, radiative and convective heating of the vehicle are of concern. However, radiative heating becomes negligible at velocities less than 6 km/sec.[24] All velocities experienced in this study are below 6 km/sec, and therefore, radiative heating is neglected. Aerothermodynamic heating is modeled using the Sutton-Graves stagnation-point convective heating equation.[25]

$$\dot{q}_{conv} = k \sqrt{\rho / r_n} \cdot v_{rel}^3 \tag{6}$$

In Equation 6, r_n is the nose radius of the vehicle and is approximated as a quarter of the vehicle's diameter for this study. The constant, k, depends on the composition of the Martian atmosphere and is 1.9027e-8 kg$^{1/2}$/cm^2.

Vehicle heating is generally mitigated with the use of an ablative TPS. The vehicle's TPS mass is estimated by the regression model based on the total heat load provided in Equation 7.[26]

$$m_{TPS} = m_0 \cdot 0.091 \left(q_{conv,total} \right)^{0.51575} \tag{7}$$

4. Payload

Applying the above definitions, the payload of the spacecraft is defined as the mass remaining once the above system masses are subtracted from the vehicle's landed mass.

$$m_{payload} = m_{landed} - \left(m_{propsys} + m_{RCS\ sys} + m_{FBS} + m_{backshell} + m_{TPS}\right) \tag{8}$$

C. Reference Mission

The current study considers two entry options: direct entry from a hyperbolic approach trajectory and entry from orbit. In the direct entry case, the simulation is initiated at a 400 km altitude with an inertial velocity of 5.85 km/sec, a state that is equivalent to 6 km/sec at atmospheric interface (altitude of 125 km). The initial flight path angle of the vehicle is optimized with respect to the mission's overall propellant mass fraction (PMF). In the entry-from-orbit cases, the vehicle is initially assumed to be in a 400 km altitude circular orbit (inertial velocity of 3.36 km/sec). The vehicle performs a deorbit maneuver to change its velocity and flight path angle. Once again, the magnitude of the deorbit burn is optimized with respect to overall PMF. Once the spacecraft has begun its descent sequence, there are no deployments, separations, or changes in configuration. The vehicle follows a ballistic trajectory, relying only on propulsion and drag for deceleration. All trajectories end with a constant-thrust gravity turn that is performed at maximum thrust and initiated at a time consistent with the vehicle T/W. The reference trajectory deceleration is performed through only aerodynamic drag and this terminal gravity turn maneuver.

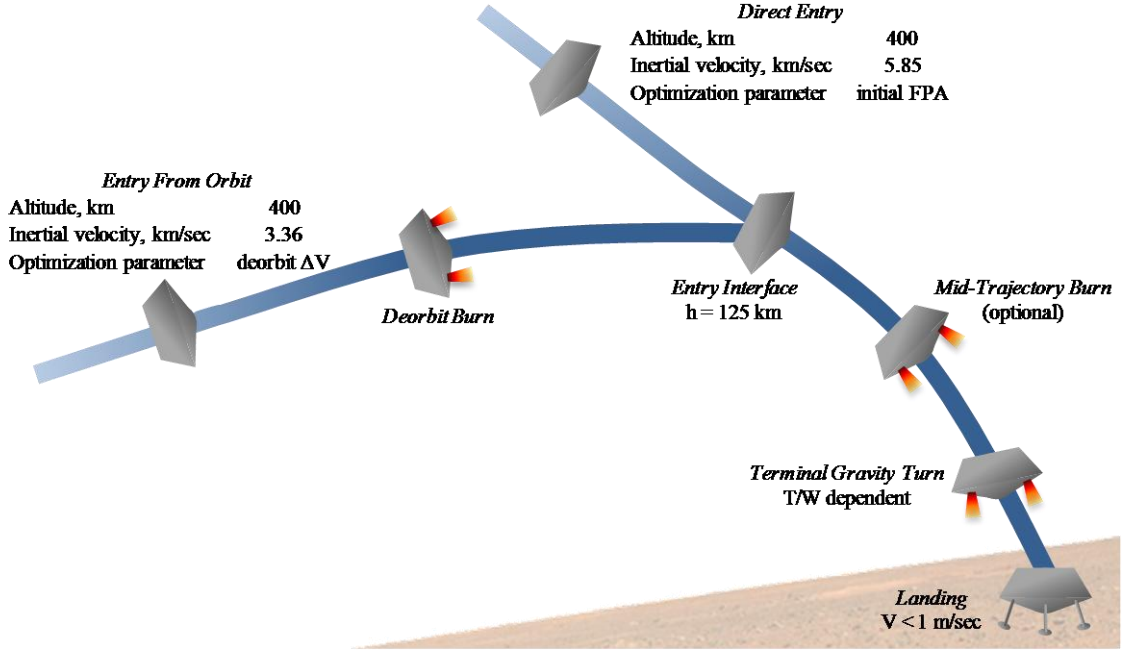

Fig. 4 Fully-Propulsive Entry, Descent, and Landing Sequence of Events

Throughout the EDL sequence, there are various constraints that must be satisfied. First, the landing conditions must be met. In order to ensure a soft landing, a Newton-based solver is used to calculate the altitude of the initiation of the terminal deceleration phase which is dependent on the vehicle's T/W. During terminal descent, the constant-thrust gravity turn is employed to arrive at the targeted surface elevation within 1 m and at less than 0.01 m/sec. In the reference trajectory, no additional ΔV is provided for a constant velocity, vertical descent segment or divert maneuver that may ultimately be required. A maximum g-limit constraint is also placed on the trajectories. Due to an expected astronaut deconditioning period on the order of 6 to 9 months, the maximum g-load constraint is set to 5 Earth g's. A heat rate constraint is also placed on the trajectories to determine if the ablative thermal protection system employed by current robotic missions can be reduced through the use of propulsion early in the trajectory. The g-limit and heat rate constraints are not implemented in the reference trajectories but are used later in this study.

III. Results

A. Reference Trajectories

As a benchmark for this investigation, reference trajectories for both the direct entry and entry-from-orbit scenarios are first established. The vehicle used for these reference cases is described in Table 4. The provided mass, ballistic coefficient, and T/W are for the vehicle at the initiation of the from-orbit or direct descents. Note that deceleration is accomplished without aeroassist technology elements such as lifting configurations, parachutes, or inflatable aerodynamic decelerators.

Table 4 Baseline Vehicle Parameters

Baseline Vehicle	
Initial mass, mT	60
Vehicle diameter, m	10
Ballistic coefficient, kg/m^2	477.5
Initial T/W	3
I_{sp}, sec	350

The entry-from-orbit reference case uses the mass-optimum deorbit ΔV, while the direct entry reference case begins with the mass-optimum initial flight path angle. At the end of each of these trajectories, a constant-thrust terminal gravity turn is used to ensure a safe landing. For the majority of the descent, the vehicle is not under power. The reference trajectories are outlined in Fig. 5 and Table 5. No in-flight constraints are considered in these two reference cases. Therefore, the mass optimization finds an initial state of the vehicle which maximizes drag throughout the trajectory. This strategy minimizes the ΔV required by the terminal gravity turn.

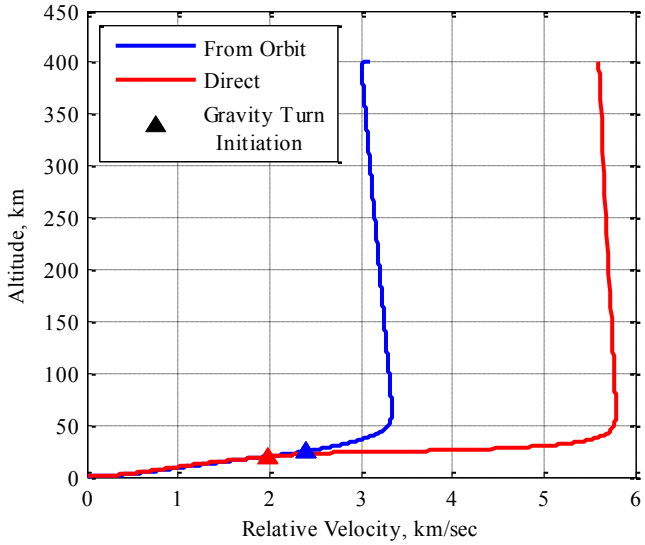

Fig. 5 Reference Trajectories

Table 5 Events and Parameters of the Reference Trajectories

Event	From Orbit	Direct
Simulation Initiation		
Time (s)	-2176	-167
Altitude (km)	400	400
Relative Vel. (km/s)	3.091	5.601
Relative FPA (°)	0.00	-21.99
Entry Interface		
Time (s)	0	0
Altitude (km)	125	125
Relative Vel. (km/s)	3.28	5.76

Relative FPA (°)	-2.92	-11.49
Gravity Turn Initiation		
Time (s)	740	295
Altitude (km)	24.3	19.1
Relative Vel. (km/s)	2.390	1.987
Relative FPA (°)	-4.18	-3.27
Trajectory Termination		
Time (s)	878	424
Altitude (km)	0	0
Relative Vel. (km/s)	0	0
Relative FPA (°)	-84.61	-86.25
Parameter		
Peak Heat Rate (W/cm^2)	7.66	48.89
Total Heat Load (J/cm^2)	2108	5837
Peak g-Load (Earth g's)	2.17	2.92
Peak Dyn. Pressure (Pa)	5490	13608
Propellant MF (%)	47.65	41.95
Payload MF (%)	14.66	16.00

B. Addition of a Heat Rate Constraint

This study explores the possibility of reducing or eliminating the entry system TPS by flying a heat rate constrained trajectory. Assuming the system is in radiative equilibrium, the heat rate limit can be computed for a given structural material by assigning a maximum allowable temperature in Equation 9.

$$\dot{q}_{conv} = k\varepsilon T^4 \tag{9}$$

In Equation 9, T temperature of the surface of the vehicle's forebody in Kelvin, k is the Stefan-Boltzmann constant (5.67 x 10-8 W/m^{2}K^4), and ε is the emissivity of the forebody material. Assuming a maximum heat rate of 1 W/cm^2 and an emissivity of 0.8, the surface temperature of the forebody at the stagnation point is computed as approximately 415°C. This represents a significant decrease in the peak temperatures of 850°C and 1540°C experienced by the entry-from-orbit and direct entry reference trajectories respectively. An argument can be made that the TPS may be eliminated for sufficiently low peak heat rates, however, there is no such assumption made in the current study. Limiting the peak heat rate reduces the total heat load during the trajectory, resulting in a lower TPS mass calculated by Equation 7. To fly a heat rate constrained trajectory, a mid-trajectory burn (MTB) is included in the EDL sequence. This additional propulsive maneuver increases the vehicle's propellant mass fraction. However, by slowing the vehicle at the right point in the trajectory, the peak heat rate can be drastically reduced. Therefore, it may be possible to reduce, or even eliminate, the mass, complexity, and cost of an ablative TPS.

The mid-trajectory propulsive maneuver was first designed as a constant-thrust burn. As with a gravity turn, the thrust was directed in the opposite direction of the velocity. An optimization of landed mass was performed using three design variables: the altitude at which the mid-trajectory burn was initiated, the burn ΔV, and the thrust magnitude of the burn. This burn was performed at constant thrust, but unlike the gravity turn, it was not necessarily performed at maximum thrust. Reducing the thrust magnitude of the mid-trajectory burn allowed for longer burn times thus controlling the vehicle's velocity over an extended period of the trajectory. This proved necessary to meet lower peak heat rate constraints; once the propulsive maneuver terminates, the vehicle accelerates due to gravity, often breaching the heating constraint.

The mid-trajectory burn acts to slow the vehicle before the heating constraint is violated. Not only does this maneuver require propellant, but the decrease in velocity also greatly reduces the deceleration due to drag. Furthermore, the vehicle's drag is reduced due to aero-propulsive effects. Example trajectories utilizing the constant-thrust mid-trajectory burn and their respective propellant mass fractions are provided in Fig. 6. For these trajectories, the mid-trajectory propulsive maneuver was initiated at the 1 W/cm^2 heat rate constraint and was performed at throttle settings of 100, 75, and 50%. The length of the burn (ΔV) was specified as to ensure that the heat rate constraint was not violated during the coast phase after the MTB was terminated. As seen in Fig. 6, the

more mass-optimal trajectories are those that are nearer to the constraint for longer periods of time. There are three reasons for this:

(1) Mid-trajectory burns with lower throttle settings require less ΔV during this segment of the trajectory. This is the result of terminating the MTB at a lower altitude. Upon termination, the vehicle has less altitude to accelerate and therefore less velocity to remove during the terminal gravity turn maneuver.

(2) Trajectories closer to the constraint experience more drag. At every altitude (or density), the vehicle is at a higher velocity resulting in a larger drag force.

(3) Lower throttle settings experience less aero-propulsive drag degradation. The lower throttle settings reduce thrust coefficient resulting in drag coefficient multipliers closer to 1 as calculated in Equation 4.

For the above reasons, it is advantageous to use the minimum thrust level required to meet the heat rate constraint resulting in a heat-rate-riding portion of the trajectory. This requires a variable thrust (throttling) method for the mid-trajectory burn.

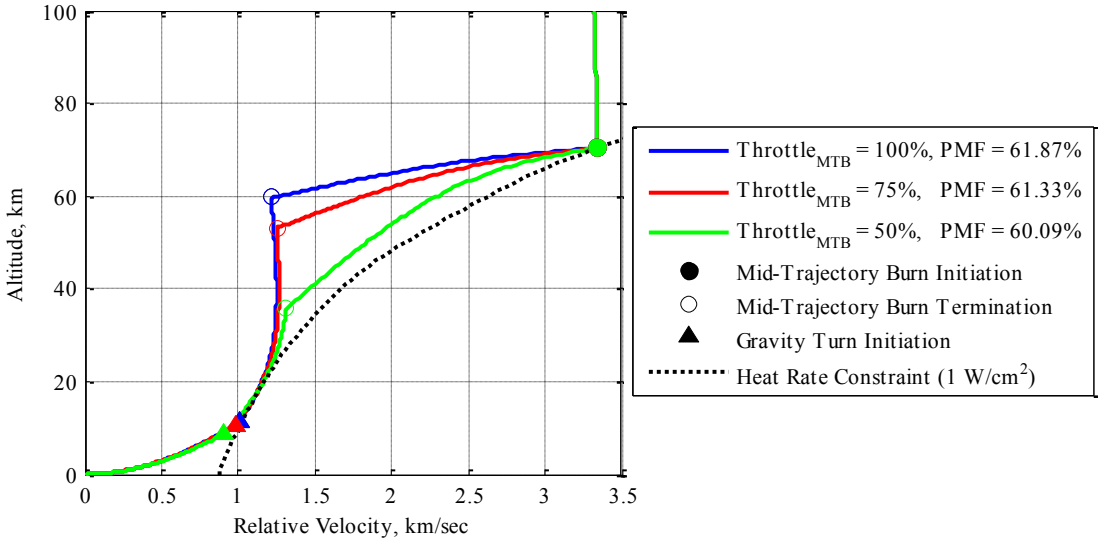

Fig. 6 Trajectories Using a Constant-Thrust Mid-Trajectory Burn

C. Mid-Trajectory Propulsive Maneuvers with Variable Thrust

Assuming knowledge of the vehicle's altitude at all times during the trajectory and an accurate model of the Mars atmosphere, the desired velocity of the spacecraft during the mid-trajectory burn can be calculated by re-arranging the Sutton-Graves stagnation-point convective heating equation into the form shown in Equation 6. Due to the previous optimality argument, defining the heat rate constraint defines the preferred trajectory of the vehicle during this phase of flight.

$$v_{rel,con} = \left(\frac{\dot{q}_{conv} \sqrt{r_n / \rho}}{k} \right)^{1/3} \tag{10}$$

Assuming that the thrust and drag forces dominate during propulsive maneuvers, the time derivative of the spacecraft velocity can be estimated through Equation 11 where T and D are the thrust and drag forces.

$$\frac{d\vec{v}_{rel}}{dt} = \frac{\vec{T} + \vec{D}}{m} \tag{11}$$

During the mid-trajectory burn maneuver, thrust and drag are directed in the opposite direction of the velocity vector, allowing for a simplification of the thrust and drag vectors in Equation 8. Through discretization, Equation 12 can be formulated from Equation 11.

$$\Delta\vec{v}_{rel} = -\Delta t \frac{T+D}{m}\hat{v}_{rel} \tag{12}$$

In Equation 12, Δv_{rel} is defined as the difference between the actual relative velocity and the desired relative velocity with respect to the heat rate constraint. The Δv_{rel} term can be thought of as the necessary change in velocity to place the vehicle on the heating constraint.

$$\Delta\vec{v}_{rel} = \vec{v}_{rel} - \vec{v}_{rel,con} \tag{13}$$

Substituting into Equation 12 and solving for thrust gives the following control law.

$$T = -\left(\frac{m\left(v_{rel} - v_{rel,con}\right)}{\Delta t} - D\right)\hat{v}_{rel} \tag{14}$$

Due to its dependence on information from the previous time step, the controller described above lags the system; the thrust calculated is that necessary to correct the velocity of the previous time step. However, with a sufficiently small time step, the lag of the controller is negligible and the spacecraft closely follows the contour provided by the heat rate constraint.

With the variable-thrust control law, the entry-from-orbit and direct entry reference trajectories are re-simulated with an assumed peak heat rate constraint of 1 W/cm^2. As shown in Fig. 7 and Table 6, both trajectories ride the heat rate constraint for a considerable portion of the descent. When mass sizing is performed on the direct entry case, a negative payload is calculated as a result of the large PMF (nearly 76%), and the case is deemed infeasible.

While the entry-from-orbit case is able to begin the mid-trajectory burn when the vehicle reaches the heat rate constraint, the direct entry must begin the burn exo-atmospherically. Due to the increased velocity of the direct entry, the vehicle would reach the heat rate constraint along a much flatter region of the constraint. As the constraint becomes more horizontal (i.e. at higher velocities), greater changes in velocity are required for the same change in altitude. To meet the constraint, the vehicle needs to increase thrust or direct its thrust in the vertical direction. (Lift may be used for this purpose, but it is not applied in this study. Incorporation of lift is considered future work.) For this study, the thrust magnitude is limited by a specified T/W, and the direction of thrust is always defined in the opposite direction of the vehicle's velocity. The remaining option for meeting the heat rate constraint for high velocity cases is starting the mid-trajectory burn earlier in the trajectory. This allows for decreases in velocity before reaching denser regions of the atmosphere where sufficient heating occurs. The portion of the mid-trajectory burn executed prior to reaching the heat rate constraint is performed at maximum thrust to limit losses. Within the simulation, the altitude at which to begin this burn is explicitly calculated so that the resulting vehicle trajectory is tangent to the heat rate constraint when the two intersect. At this point, the thrust is throttled according to the control law provided by Equation 14. After some time riding the heat rate constraint, drag provides enough deceleration so that thrust is no longer required to meet the constraint. In many trajectories, this results in a period of no thrust between the mid-trajectory burn and the final gravity turn maneuver. As shown in Table 6 for the case of a 1 W/cm^2 constraint, this non-thrusting phase of flight spans a relatively small range of altitudes. These behaviors are shown in Fig. 7 and Fig. 8.

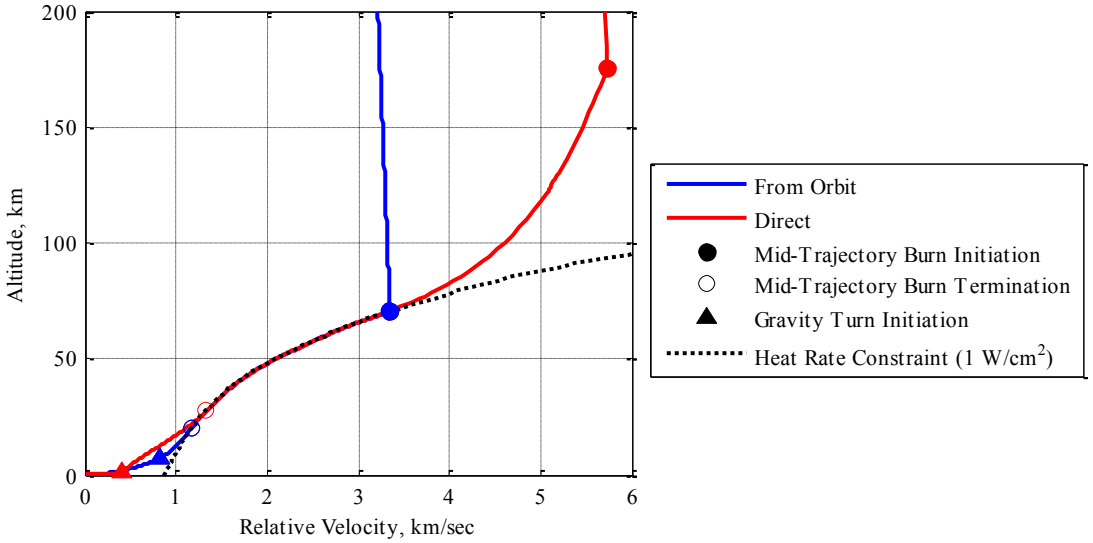

Fig. 7 Baseline Vehicle Employing a Variable-Thrust Mid-Trajectory Burn

Table 6 Events and Parameters of Trajectories Employing Mid-Trajectory Burns

Event	From Orbit	Direct
Simulation Initiation		
Time (s)	-2448	-193
Altitude (km)	400	400
Relative Vel. (km/s)	3.091	5.599
Relative FPA (º)	0.00	-20.68
Entry Interface		
Time (s)	0	0
Altitude (km)	125	125
Relative Vel. (km/s)	3.291	5.123
Relative FPA (º)	-2.15	-8.84
Mid-Traj. Burn Initiation		
Time (s)	664	-52
Altitude (km)	70.4	175.5
Relative Vel. (km/s)	3.340	5.723
Relative FPA (º)	-0.61	-11.91
Mid-Traj. Burn Termination		
Time (s)	1043	255
Altitude (km)	20.4	27.6
Relative Vel. (km/s)	1.173	1.323
Relative FPA (º)	-16.21	-14.20
Gravity Turn Initiation		
Time (s)	1082	345
Altitude (km)	7.2	1.2
Relative Vel. (km/s)	0.830	0.399
Relative FPA (º)	-23.04	-35.27
Trajectory Termination		
Time (s)	1119	355
Altitude (km)	0	0
Relative Vel. (km/s)	0	0
Relative FPA (º)	-80.38	-70.72
Parameter		

Peak Heat Rate (W/cm^2)	1.00	1.00
Total Heat Load (J/cm^2)	646	251
Peak g-Load (Earth g's)	2.84	4.71
Peak Dyn. Pressure (Pa)	2951	1804
Propellant MF (%)	59.95	75.86
Payload MF (%)	4.25	-11.58

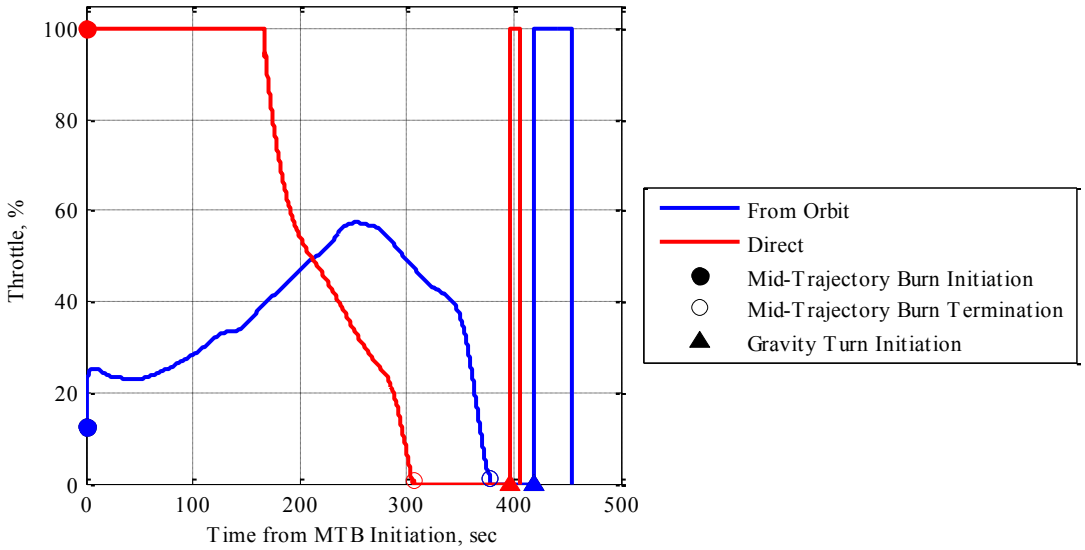

Fig. 8 Control History for the Baseline Vehicle Employing a Variable-Thrust Mid-Trajectory Burn

D. Mass Sizing

To study the impact of a fully-propulsive descent on mission capability, the payload mass fraction is calculated using the sizing methodology outlined earlier in this report. For comparison, the mass breakdowns of the baseline vehicle for the reference trajectory from orbit as well as the fully-propulsive descent with a heat rate constraint of 1 W/cm^2 are provided in Table 7. As expected, the fully-propulsive descent system sees a significant increase in necessary propellant. The added propellant requires larger propellant tanks resulting in additional mass growth. In this case, the mass benefit of reducing the TPS mass is overshadowed by the increase in propellant and propellant tank mass, resulting in a drastically lower payload mass fraction.

Table 7 Mass Breakdown of the Baseline Vehicle for the Entry-From-Orbit Case

	Reference Trajectory	**Fully-Propulsive (1 W/cm^2)**
	% of Initial Mass	
Propulsion System	*56.53*	*70.11*
Propellant	47.65	59.95
Engines	1.94	1.94
Propellant Tanks	4.93	6.20
RCS Hardware	0.50	0.50
RCS Propellant	1.52	1.52
Structure	*24.10*	*23.08*
Forebody	10.10	9.08
Backshell	14.00	14.00
TPS	*4.71*	*2.56*
Payload	*14.66*	*4.25*

E. Sensitivity Analysis

To identify and further understand the key parameters of a fully-propulsive EDL sequence, sensitivity analysis was performed. This analysis investigated the impact of propulsive system performance, aero-propulsive effects, structure models, initial mass, and heat rate limit on payload delivered to the surface of Mars.

1. Propulsion Performance

To investigate the sensitivity of payload mass to propulsive system performance, the vehicle's thrust to weight ratio and specific impulse are varied from 2 to 10 and 250 to 1250 sec, respectively. The analysis was performed on the baseline vehicle utilizing a variable thrust mid-trajectory burn with a heat rate constraint of 0.5 W/cm^2.

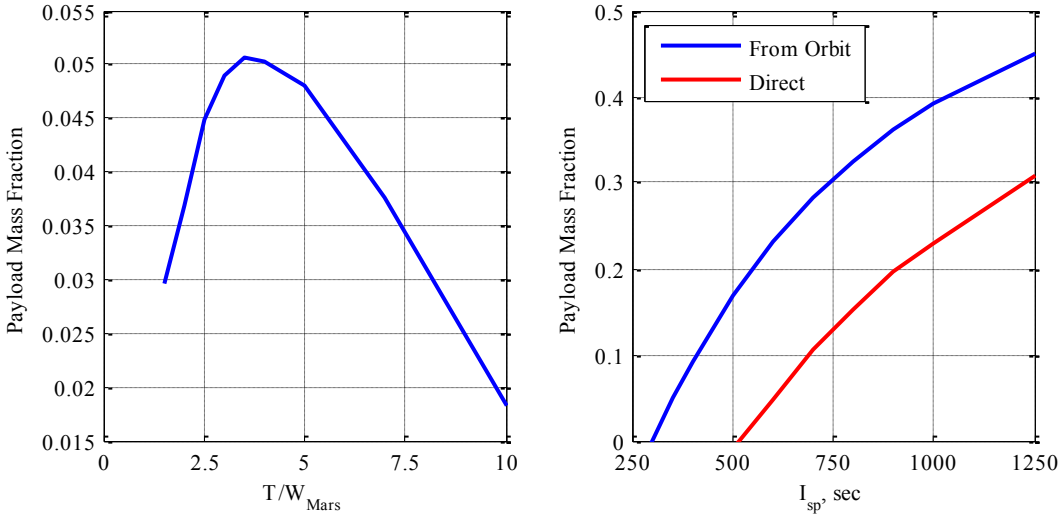

Fig. 9 Propulsion System Capability Sensitivity Analysis

Contrary to the results shown in Fig. 3, the vehicle's thrust to weight ratio has negligible impact on the overall propellant mass fraction for heat-rate limited entries, since the mid-trajectory burn is not generally performed at maximum thrust. In the trajectories computed, the mid-trajectory burn ΔV is approximately three times as large as the terminal gravity turn ΔV. Therefore, the benefit of having a larger maximum thrust available is not fully realized. Note that improvements in vehicle T/W do not enable heat rate constrained direct entries.

Further exploration of the data shows that bounds can be set on the required T/W based on the heat rate and g-load constraints. The heat rate constraint defines the lower boundary of the thrust to weight ratio. In the current control structure, the vehicle must have the ability to travel along the heat rate constraint for a significant portion of the trajectory. For the constraints and trajectories examined in this study, the lower bound on the required T/W can be approximated as 2.5. For lower thrust to weight ratios, the mid-trajectory burn must be started earlier in the trajectory resulting in higher propellant needs. The upper bound of the vehicle's thrust to weight is determined by the allowable g-load constraint. For 5 Earth g's, the maximum Mars thrust to weight ratio can be calculated as approximately 13. However, use of maximum thrust at this T/W would result in breaching the g-load constraint due to additional deceleration due to drag (maximum of 1.5 g's for the cases examined in this study). As such, a conservative maximum T/W on the order of 10 is appropriate. The optimum shown in Fig. 9 occurs at a T/W of 3.5. The optimum occurs as a result of balancing the increased efficiency of higher thrust burns and the increased engine mass necessary for that higher thrust.

Unlike thrust to weight ratio, the vehicle's specific impulse has significant impact on the overall propellant mass fraction and, consequently, delivered payload. The range of specific impulses included in this study is expanded beyond the current technological limits to include hypothetical engines such as nuclear thermal rockets. As can be seen in Fig. 9, increasing I_{sp} greatly impacts payload mass fraction. The previously infeasible direct entry is enabled once the I_{sp} becomes greater than 500 sec. Important to note for specific impulses of 470 sec and 890 sec respectively, the entry-from-orbit and direct entry cases deliver equivalent payload as the reference trajectory.

2. Aero-Propulsive Effects and Structural Modeling

In an effort to examine the impact of the aero-propulsive effects and structural modeling on delivered payload, a study was conducted in which the baseline models were altered. The aero-propulsive effect model given in Equation 4 was replaced with a simple percent multiplier. As shown in Fig. 10, the baseline vehicle entering from orbit retains approximately 50% of its overall drag with the original model. From the analysis, it is seen that the development of retropropulsion configurations which maintain drag could lead to relatively significant increases in delivered

payload. To examine the impacts of structural modeling, the mass fraction assigned to backshell mass was changed. As can be seen in Fig. 10, reductions in structural mass fraction directly translate to higher payload mass fractions. Unfortunately, retropropulsion configurations and lightweight structures by themselves do not enable direct entries.

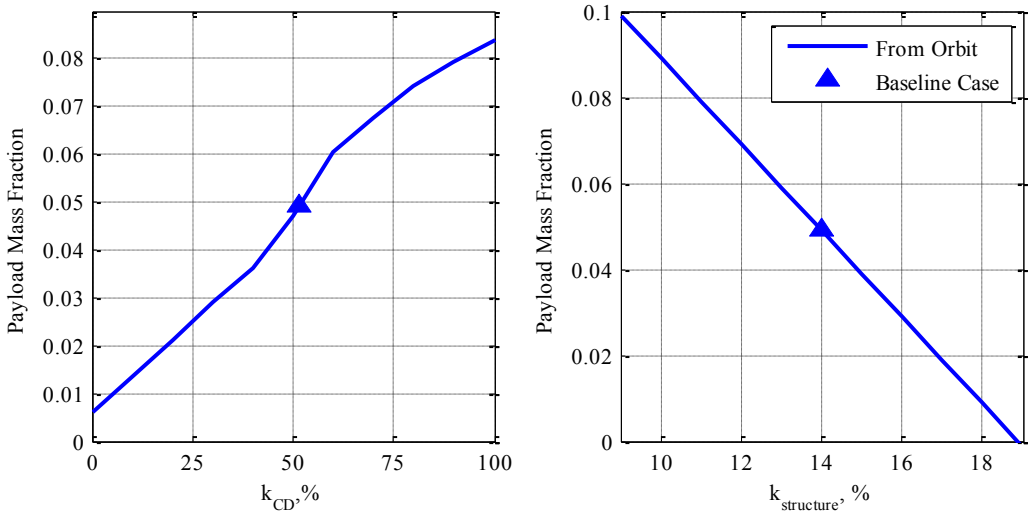

Fig. 10 Aero-Propulsive Effects and Structural Modeling Sensitivity Analysis

3. Initial Mass and Heat Rate Constraint

To further examine the sensitivity to the heat rate constraint, a series of cases were simulated. These cases included heat rate constraints ranging from 0.1 to 10 W/cm^2 and initial masses spanning 20 to 100 mT. The results of this study are presented in Fig. 11 for both entry-from-orbit cases and direct entry cases. As seen in the plots, the payload mass fraction increases as the heat rate constraint is relaxed. This is expected as a higher heat rate constraint allows for more deceleration due to drag and, therefore, less propellant use throughout the trajectory. Due to required TPS mass for higher heat rates, there is a region of cases (heat rate constraints of 2-3 W/cm^2, initial masses greater than 80 mT) which are outperformed by lower heat rates. This result suggests that using propulsion to only mitigate and not eliminate heating concerns for these cases is inefficient. Fig. 11 also shows the tendency to limit the magnitude of the mid-trajectory burn through the initial trajectory optimization. The extreme of this trend is shown as the 5, 7, and 10 W/cm^2 contours merge as the initial mass decreases. These trajectories require no mid-trajectory burn to adhere to the heat rate constraint, and therefore, fly trajectories similar to that of the reference case.

Beyond the sensitivity to the heat rate constraint, Fig. 11 shows the feasibility limits of the current fully-propulsive descent architecture. Cases are deemed infeasible if the mass sizing algorithm assigns a negative payload mass fraction. In the scope of the study presented here, the entry-from-orbit cases become infeasible for the 100 mT cases which have heat rate constraints of 0.1, 2, and 3 W/cm^2. The 0.1 W/cm^2 heat rate is too stringent and requires too much propellant; whereas, the 2 and 3 W/cm^2 cases require significant TPS mass as well as propellant. The direct entry cases are considerably more difficult and therefore result in many more failed cases. As seen in Fig. 11, all cases with heat rate constraints less than 2 W/cm^2 are infeasible. By comparing the two plots, it can be seen that a direct entry's payload mass fraction is approximately 15-30% less than a corresponding entry-from-orbit case. Therefore, it may be concluded that fully-propulsive descent strategies are best implemented from orbit.

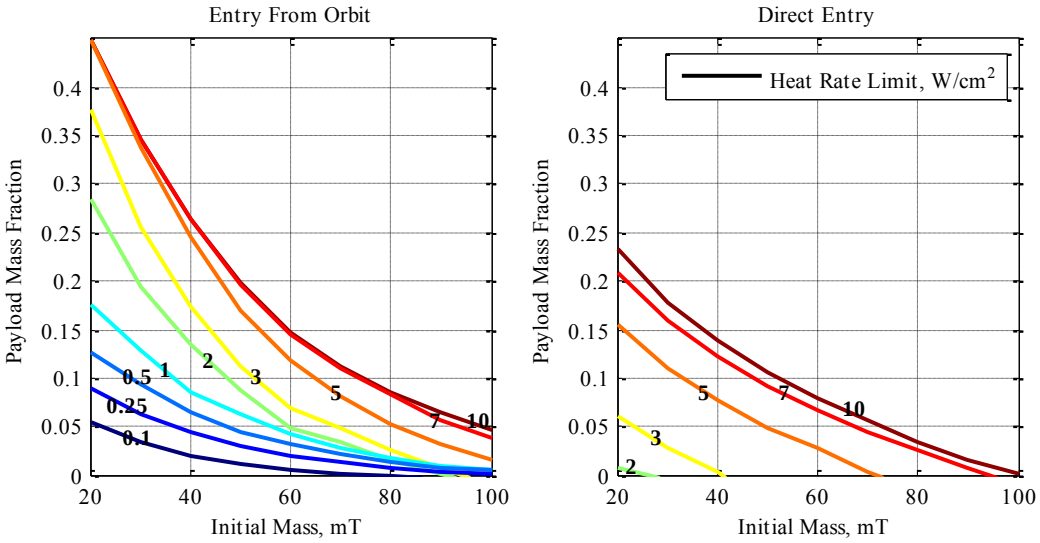

Fig. 11 Initial Mass and Heat Rate Constraint Sensitivity Analysis

F. Comparison with Aeroassist EDL Systems

In an effort to compare the fully-propulsive descent against a more traditional aeroassist EDL system, Table 8 is offered. As expected, the fully-propulsive descent recognizes significant decreases in peak heat rate, total heat load, and peak dynamic pressure at the expense of propellant and subsequently payload. The suggested 1 W/cm^2 heat rate constrained case is greatly outperformed by the aeroassist system. However, by easing the constraint to 5 or 7 W/cm^2, the gap in performance is narrowed slightly. As seen in Table 8, the fully-propulsive descent requires some form of technology advancement to become competitive with aeroassist strategies.

Table 8 Comparison between Aeroassist and Fully-Propulsive EDL Systems

	From Orbit			
	Fully-Propulsive Descent			*CUIP*[18]
	1 W/cm^2	5 W/cm^2	7 W/cm^2	Lifting, IAD
Peak Heat Rate (W/cm^2)	1.00	5.00	7.00	19.18
Total Heat Load (J/cm^2)	646	2791	2293	5018
Peak g-Load (Earth g's)	2.84	2.26	2.18	7.88
Peak Dyn. Pressure (Pa)	2951	5009	5265	49996
Propellant MF (%)	59.95	49.70	47.74	10.62
Payload MF (%)	4.25	11.82	14.42	43.23

G. Mission Impact

Introduction of the fully-propulsive descent can significantly impact the dynamics and requirements of the EDL segment from a mission architecture, complexity, and reliability perspective.

1. Mission Architecture

Implementing a fully-propulsive descent during the EDL segment of a mission will impact the overall mission architecture. From the above analysis, a heat-rate limited direct entry requires a large propellant mass fraction which significantly decreases or eliminates the payload delivered to the Mars surface. As shown in this investigation, fully-propulsive descents are best implemented from orbit. Once entry-from-orbit is selected, an appropriate method for orbit insertion must be determined. Due to the availability of a capable propulsion system, propulsive insertion may be possible. The propulsive maneuver to transfer the vehicle from the hyperbolic approach to the 400 km altitude circular orbit requires a ΔV of approximately 2.5 km/sec. This results in a propellant mass fraction on the order of 50% for the orbit insertion burn. If all of the needed propellant is to be transported from Earth, the baseline vehicle with a mass of 60 mT in Mars orbit grows to over 350 mT at Earth departure. However, an in-situ supplied propellant depot in Mars orbit would allow a mission architecture in which the spacecraft refuels after insertion into Mars orbit.[28] Also, significant improvements in Earth launch mass can be realized if propellant depots are available

in low-Earth orbit as well. Fig. 12 outlines the mass of the vehicle from Earth launch to touchdown on the surface of Mars. The mission assumes propellant resources in both Earth and Mars orbit and that both the Earth-departure burn and Mars orbital insertion burn are performed by the vehicle. This mission architecture requires a 25 mT launch mass to land 2.55 or 8.65 mT of payload on the surface of Mars for fully-propulsive EDL sequences that have 1 and 7 W/cm^2 heat rate constraints respectively.

Another orbit insertion option at Mars is aerocapture. This maneuver is suggested by Christian et al.[19] A similar orbit insertion maneuver is possible for the current study. If paired with refueling at Mars, the fully-propulsive descent allows for a much lower mass aerocapture system (a baseline vehicle with a mass of approximately 25 mT). After the aerocapture maneuver, the vehicle can rendezvous with the propellant depot and take on the fuel needed for the fully-propulsive descent. Due to the addition of a heatshield needed for aerocapture, this orbit insertion method increases the launch mass required. However, aerocapture greatly decreases the amount of propellant used in Mars orbital insertion and Earth departure.

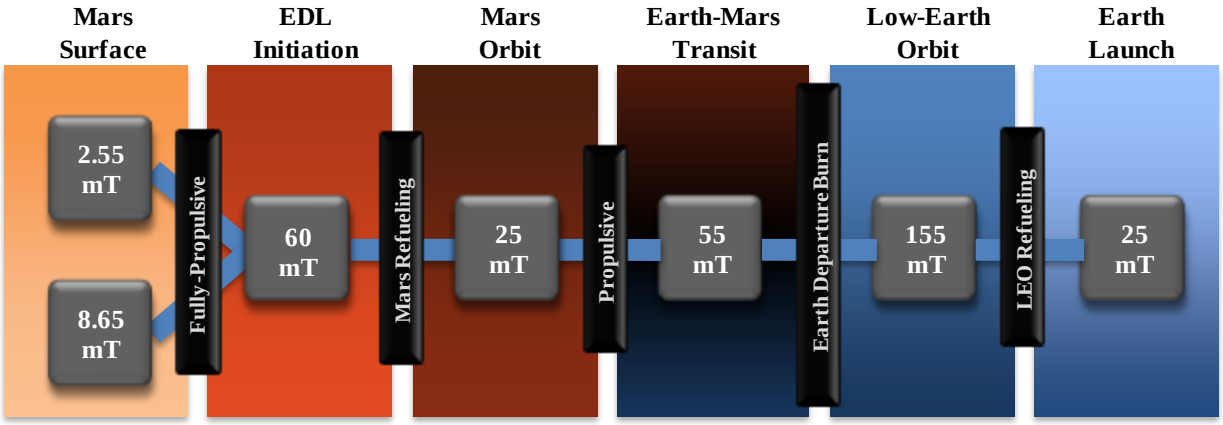

Fig. 12 Fully-Propulsive EDL Mission Architecture

Finally, the lack of dependency on aerodynamic forces places less of a demand on shaping the aeroshell for those purposes. Although not examined in this study, a fully-propulsive descent allows for more flexibility in the shape of the vehicle. This in turn lets the vehicle be designed for surface operations instead of survival of EDL. The vehicle can be designed with a larger habitable volume, easier entry and egress systems, or compatibility with prepositioned surface assets. The increased functionality of the vehicle may lead to a simpler and more productive surface operations phase.

2. *Complexity*

To analyze the effect of a fully-propulsive descent on the complexity of a mission, it is appropriate to analyze both hardware and operations. As offered in this study, a fully-propulsive descent may be used to avoid harsh heating environments usually encountered in atmospheric transit. In this light, the difficulty of developing and employing an enhanced propulsion system is being traded for that of TPS. The performance of the propulsion system greatly impacts the feasibility of the proposed EDL sequence. The specific impulse of 350 sec assumed in this study is widely accepted for LOX/CH_4 engines, and the thrust assumed for the baseline vehicle is approximately 700 kN (less than half of the thrust produced from one of the Space Shuttle's main engines). Throttling authority allows for added control of the vehicle and enables the heat rate limited trajectories which allow elimination of the TPS. However, throttling of high-performance rocket engines is not easily achieved. The continuous throttling ability assumed in this study would likely be implemented as a series of discrete throttle settings at a small cost to performance.

Other concerns of the fully-propulsive descent sequence include thrusting into a hypersonic flow. Research focused on supersonic retropropulsion has examined thrusting into flows with Mach numbers up to 6;[21] however, thrusting into flows with Mach numbers of up to 25 occurred in this study.

The difficulties of a fully-propulsive descent must be compared against those of a more conventional EDL sequence which relies on aeroassist strategies. One driver of complexity in an aeroassist trajectory is the reconfiguration of the vehicle during descent. These events often include the separation of the heatshield and backshell, deployment of a parachute or IAD, possible banking maneuvers for lifting trajectories, the use of novel aeroshell geometries for improved aerodynamic control authority, and a terminal thrusting maneuver. During an aeroassist trajectory, certain flight conditions must be met in order to successfully complete each of these events. For

instance, a parachute or IAD must be deployed in a specific Mach and altitude envelop. These requirements are not present for a fully-propulsive descent.

Another source of complexity for an aeroassist trajectory is the development of the vehicle's TPS. This issue becomes increasingly difficult as the vehicle grows in size. Growth of the vehicle leads to paneling or tiling of the TPS material. Due to the limits in the size of individual panels or tiles, the quantity of the pieces needed to properly protect the vehicle increases as well as the number of seams between those pieces. This leads to increased risk and complexity as the vehicle becomes larger.

3. Reliability

In much the same way as complexity, reliability of a fully-propulsive descent can be compared against aeroassist EDL sequences. Of major concern would be the ability to initiate a large rocket engine after being dormant for a six to nine month transit period. However, this issue is present for many robotic deep space missions and is solved by focusing on engine reliability.

An increase in reliability of the fully-propulsive descent can also be realized if a divert capability is included in the EDL sequence. Divert maneuvers could be used during EDL to increase landing reliability by providing the ability to reach multiple landing sites. Diverting requires propulsive maneuvers at the end of a trajectory. For the case of an aeroassit trajectory, a divert maneuver must begin after parachute or IAD separation.[27] For a fully-propulsive descent, the divert maneuver may start at any point in the trajectory. This would increase the possible landing area thereby increasing the number of landing sites available or the range of abort-to-the-surface options.

IV. Future Work

During the course of the current study, the authors identified several areas which warrant further examination.

Lifting Trajectories – The use of lift, especially during heat rate guided trajectories, may have significant impact on the required propellant mass fraction. Constant or near-constant altitude deceleration would allow for following the prescribed heat rate constraint. Lift modulation would need to be incorporated into the current control scheme. Lift may be augmented with thrust in cases where lift alone cannot meet the heat rate constraint.

Guided Descent – Fully-propulsive descent provides significant control authority throughout the EDL sequence. Benefits may be realized by earlier guidance initiation, increased divert options, and ability to land at higher altitudes.

Optimal Control – The problem of heat rate limited trajectories can be approached from an optimal control perspective. These efforts should be focused on proving the optimality of the heat-rate-riding strategy and examine thrust directions not aligned with the velocity vector.

Conceptual Vehicle Configuration – Creative effort should be invested in developing a conceptual vehicle configuration. This work would aim to answer the general question "What does the vehicle look like?" The work should include atmospheric transit, landing, and surface configurations.

V. Conclusions

This study has explored the use of propulsion during the EDL sequence at Mars for high-payload missions. The study focused on replacing conventional aeroassist EDL strategies with one that relies solely on propulsion. For the study, trajectory simulation and mass sizing were performed to analyze the feasibility of a fully-propulsive descent. A heat rate boundary and associated control law were developed in an effort to limit the heating loads placed on the vehicle. The results show that the fully-propulsive descent strategy is best implemented after the vehicle has been inserted into Mars orbit due to the high propulsive requirements and inability to refuel in Mars orbit during a direct entry. The fully-propulsive transit architecture provides low payload mass fractions (less than 10%) without significant improvements in I_{sp} or the vehicle's aero-propulsive model at high thrust coefficients. These values are much lower than the 20-30% payload mass fractions suggested by more traditional Mars EDL strategies. When coupled with refueling resources in Earth and Mars orbit, a fully-propulsive EDL strategy can deliver 8.65 mT of payload to Mars with Earth-launch masses as low as 25 mT.

To enable high payload missions to Mars, conventional aeroassist strategies require further technology development in multiple areas such as TPS, inflatable aerodynamic decelerators, supersonic parachutes, and aeroshell configurations; whereas, a fully-propulsive descent strategy would require technology advancements in

high-thrust, high-I_{sp} propulsion systems, drag-preserving retropropulsion configurations, and lightweight structural materials.

Acknowledgements

The authors would like to thank the students and faculty of the Space Systems Design Laboratory at the Georgia Institute of Technology, especially Ian Clark, Michael Grant, Ashley Korzun, and Bradley Steinfeldt.

References

[1]Braun, R.D. and Manning, R.M., "Mars Exploration Entry, Descent, and Landing Challenges," *Journal of Spacecraft and Rockets*, Vol. 44, No. 2, pp. 310-323, 2007.

[2]Prakash, R., *et al*, "Mars Science Laboratory Entry, Descent, and Landing System Overview," *2008 IEEE Aerospace Conference Proceedings*, Paper 1531, Big Sky, Montana, March 2008.

[3]"Vision for Space Exploration," NASA NP-2004-01-334-HQ, February 2004.

[4]B.G. Drake (ed.), "Reference Mission Version 3.0 Addendum to the Human Exploration of Mars: The Reference Mission of the NASA Mars Exploration Study Team," NASA/SP-6107-ADD, June 1998.

[5]Cheatham, D.C., and Bennett F.V., "Apollo Lunar Module Landing Strategy," *Apollo Lunar Landing Symposium*, June 1966.

[6]Cooley, C.G., and Lewis, J.G., "Viking Lander System Primary Mission Performance Report," NASA CR-145148, April 1977.

[7]Ingoldby, R.N., *et al*, "Entry Data Analysis for Viking Landers 1 and 2," NASA CR-159388, November 1976.

[8]Morrisey, D.C., "Historical Perspective: Viking Mars Lander Propulsion," *Journal of Propulsion and Power*, Vol. 8, No. 2, pp. 320-331, 1992.

[9]Spencer, D. A., *et al*, "Mars Pathfinder Entry, Descent, and Landing Reconstruction," *Journal of Spacecraft and Rockets*, Vol. 36, No. 3, pp. 357-366, 1999.

[10]McGrath, D.K., and Carr II, C.E., "Mars Pathfinder Retrograde Rocket Development," *34th AIAA/ASME/SAE/ASEE Joint Propulsion Conference and Exhibit*, Cleveland, Ohio, July 1998.

[11]Desai, P.N., and Knocke, P.C., "Mars Exploration Rovers Entry, Descent, and Landing Trajectory Analysis," *AIAA/AAS Astrodynamics Specialist Conference and Exhibit*, AIAA 2004-5092, Providence, Rhode Island, August 2004.

[12]Moore, C.A., and Guernsey, C., "Development and Qualification of the Rocket-Assisted Deceleration (RAD) and Transverse Impulse Rocket System (TIRS) Motors for the Mars Exploration Rover (MER)," *52nd Joint Army-Navy-NASA-Air Force (JANNAF) Propulsion Meeting*, Las Vegas, Nevada, May 2004.

[13]Grover III, M.R., Cichy, B.D., and Desai, P.N., "Overview of Phoenix Entry, Descent, and Landing System Architecture," *Proceedings of AIAA Guidance, Navigation, and Control Conference*, AIAA 2008-7213, Honolulu, Hawaii, August 2008.

[14]Prince, J.L., *et al*, "Mars Phoenix Entry, Descent, and Landing Simulation Design and Modeling Analysis," *Proceedings of AIAA Guidance, Navigation, and Control Conference*, AIAA 2008-7507, Honolulu, Hawaii, August 2008.

[15]Goldstein, B., and Shotwell, R., "Phoenix - The First Mars Scout Mission (A Mid-Term Report)," *2006 IEEE Aerospace Conference Proceedings*, Big Sky, Montana, March 2006.

[16]Powell, R.W., Striepe, S.A., Desai, P.N., and Braun, R.D., "Program to Optimize Simulated Trajectories (POST), Utilization Manual," Version 5.0, September 1996.

[17]Steinfeldt, B.A., Grant, M.J., Matz, D.M., Braun, R.D., and Barton, G.H., "Guidance, Navigation and Control Technology System Trades for Mars Pinpoint Landing," *2008 AIAA Atmospheric Flight Mechanics Conference*, AIAA 2008-6216, Honolulu, Hawaii, August 2008.

[18]Steinfeldt, B., *et al*, "High Mass Mars Entry, Descent, and Landing Architecture Assessment," *Space 2009*, AIAA 2009-6684, Pasadena, California, September 2009, (to be published).

[19]Christian, J., *et al*, "Extension of Traditional Entry, Descent, and Landing Technologies for Human Mars Exploration," *Journal of Spacecraft and Rockets*, Vol. 45, No.1, pp. 130-141, 2008.

[20]Klepikov, I.A., Katorgin, I.A., and Chvanov, V.K., "The New Generation of Rocket Engines, Operating by Ecologically Save Propellant 'Liquid Oxygen and Liquefied Natural Gas (Methane)'," *Acta Astronautica*, Vol. 41, No. 4-10, pp. 209-217, 1997.

[21]Korzun, A.M., Cruz, J.R., and Braun, R.D., "A Survey of Supersonic Retropropulsion Technology for Mars Entry, Descent, and Landing," *2008 IEEE Aerospace Conference Proceedings*, Paper 1246, Big Sky, Montana, March 2008.

[22]Jarvinen, P.O., and Adams, R.H., "The Aerodynamic Characteristics of Large Angled Cones with Retrorockets," Contract No. NAS 7-576,

[23]Humble, R.W., Henry, G.N., and Larson, W.J., *Space Propulsion Analysis and Design*, McGraw-Hill Companies, New York, 1995.

[24]Tauber, M.E., and Sutton, K., "Stagnation-Point Radiative Heating Relations for Earth and Mars Entries," *Journal of Spacecraft and Rockets*, Vol. 28, No. 1, pp. 40-42, 1991.

[25]Sutton, K., and Graves, R.A., Jr., "A General Stagnation-Point Convective-Heating Equation for Arbitrary Gas Mixtures," NASA TR R-376, November 1971.

[26]Laub, B., and Venkatapathy, R., "Thermal Protection System Technology and Facility Needs for Demanding Future Planetary Missions," *International Workshop on Planetary Probe Atmospheric Entry and Descent Trajectory Analysis and Science*, Lisbon, Portugal, October 2003.

[27]Grant, M.J. and Braun, R.D., "Smart Divert: A New Entry, Descent, and Landing Architecture," *47th AIAA Aerospace Sciences Meeting Proceedings*, January 2009.

[28]Powell, J., Maise, G., and Paniagua, J., "A Self-Sustaining Earth-Mars Architecture Utilizing Martian Colonies Based on the North Polar Cap," *2001 IEEE Aerospace Conference Proceedings*, Big Sky, Montana, March 2001.